Title

Inversion recovery ultrashort echo time imaging of ultrashort T2 tissue components in ovine brain at 3 T: a sequential D2O exchange study

Journal

NMR in Biomedicine, 30(10)

ISSN

0952-3480

Authors

Fan, Shu-Juan
Ma, Yajun
Chang, Eric Y
et al.

Publication Date

2017-10-01

DOI

10.1002/nbm.3767

Received: 19 January 2017 | Revised: 22 May 2017 | Accepted: 31 May 2017

DOI: 10.1002/nbm.3767

WILEY NMR IN BIOMEDICINE

RESEARCH ARTICLE

Inversion recovery ultrashort echo time imaging of ultrashort T_2 tissue components in ovine brain at 3 T: a sequential D_2O exchange study

Shu-Juan Fan[1] | Yajun Ma[1] | Eric Y. Chang[1,2] | Graeme M. Bydder[1] | Jiang Du[1]

[1] Department of Radiology, University of California, San Diego, CA, USA

[2] Department of Radiology, VA San Diego, Healthcare System, San Diego, CA, USA

Correspondence
J. Du, University of California, San Diego, Department of Radiology, 200 West Arbor Drive, San Diego, CA 92103-8756, USA.
Email: jiangdu@ucsd.edu

Funding information
National Institute of Neurological Disorders and Stroke, National Institutes of Health (NINDS, NIH), Grant/Award Number: 1R01 NS092650

Inversion recovery ultrashort echo time (IR-UTE) imaging holds the potential to directly characterize MR signals from ultrashort T_2 tissue components (STCs), such as collagen in cartilage and myelin in brain. The application of IR-UTE for myelin imaging has been challenging because of the high water content in brain and the possibility that the ultrashort T_2^* signals are contaminated by water protons, including those associated with myelin sheaths. This study investigated such a possibility in an ovine brain D_2O exchange model and explored the potential of IR-UTE imaging for the quantification of ultrashort T_2^* signals in both white and gray matter at 3 T. Six specimens were examined before and after sequential immersion in 99.9% D_2O. Long T_2 MR signals were measured using a clinical proton density-weighted fast spin echo (PD-FSE) sequence. IR-UTE images were first acquired with different inversion times to determine the optimal inversion time to null the long T_2 signals (TI_{null}). Then, at this TI_{null}, images with echo times (TEs) of 0.01–4 ms were acquired to measure the T_2^* values of STCs. The PD-FSE signal dropped to near zero after 24 h of immersion in D_2O. A wide range of TI_{null} values were used at different time points (240–330 ms for white matter and 320–350 ms for gray matter at TR = 1000 ms) because the T_1 values of the long T_2 tissue components changed significantly. The T_2^* values of STCs were 200–300 μs in both white and gray matter (comparable with the values obtained from myelin powder and its mixture with D_2O or H_2O), and showed minimal changes after sequential immersion. The ultrashort T_2^* signals seen on IR-UTE images are unlikely to be from water protons as they are exchangeable with deuterons in D_2O. The source is more likely to be myelin itself in white matter, and might also be associated with other membranous structures in gray matter.

KEYWORDS

gray matter, inversion recovery ultrashort echo time imaging, inversion time, myelin, T_2^*, white matter

1 | INTRODUCTION

The myelin sheath is a lipid-protein lamellar membranous structure. It envelops axons and is essential for the rapid propagation of electrical signals in the nervous system. In the human brain, myelin constitutes approximately 14% of the wet mass of white matter (WM); it is also present in gray matter (GM) in smaller quantities.[1,2] Loss of myelin integrity is an important biomarker for a variety of neurological diseases, such as multiple sclerosis (MS), which is a leading cause of disability in young and middle-aged adults.[1,3,4]

Abbreviations used: FOV, field of view; f_S, fraction of ultrashort T_2 tissue components; FSE, fast spin echo; GM, gray matter; GM_L, long T_2 tissue components in gray matter; GM_S, ultrashort T_2 tissue components in gray matter; IR-UTE, inversion recovery ultrashort echo time; ${}_LT_2^*$, T_2^* of the long T_2 tissue components; MRI, magnetic resonance imaging; MS, multiple sclerosis; NMR, nuclear magnetic resonance; PD, proton density; PD-FSE, proton density-weighted fast spin echo; RF, radiofrequency; ROI, region of interest; SNR, signal-to-noise ratio; ${}_ST_2^*$, T_2^* of the ultrashort T_2 tissue components; STCs, ultrashort T_2 tissue components; TE, echo time; $TE_{0.6ms}$, TE = 0.6 ms; $TE_{10\mu s}$, TE = 10 μs; TI, inversion time; TI_{null}, optimal inversion time for nulling long T_2 signals; UTE, ultrashort echo time; WM, white matter; WM_L, long T_2 tissue components in white matter; WM_S, ultrashort T_2 tissue components in white matter

Myelin produces extremely short-lived magnetic resonance imaging (MRI) signals, which cannot be imaged directly *in vivo* using most currently available clinical MRI sequences, which typically have echo times (TEs) of several milliseconds or longer. Several relaxometry studies have characterized T_2 distributions in brain tissue, reporting values of 10–50 ms in water associated with myelin sheaths.[5-8] Signals from these distributions are detectable with conventional clinical pulse sequences. These include T_1- and T_2-weighted fast spin echo (FSE) imaging, gadolinium-enhanced MRI, diffusion tensor imaging and magnetization transfer imaging. These techniques have all shown high sensitivity for MS lesions,[9-14] but measures obtained with these techniques have not been strongly correlated with clinical manifestations.[10-17] It is possible that this lack of correlation is because these measures cannot differentiate demyelination and remyelination from other pathological substrates, such as axonal loss and gliosis, which are associated with heterogeneous clinical manifestations of MS.[18,19] Methods for direct myelin imaging *in vivo* provide a more specific and sensitive evaluation of myelin, and thus might be of considerable value.

Previous nuclear magnetic resonance (NMR) spectroscopy studies have measured tissue myelin T_2 *ex vivo* and have reported values of approximately 50 μs in fixed human WM[13] and 50 μs to 1 ms in freshly excited frog sciatic nerve.[4] Inversion recovery ultrashort echo time (IR-UTE) sequences have the potential to selectively image short-lived MRI signals *in vivo* through the efficient suppression of long-lived water signals using an adiabatic inversion recovery pulse.[20,21] Wilhelm et al[2] first demonstrated IR-UTE imaging of myelin signals in excised rat spinal cord on a 9.4-T microimaging system. A more recent study explored the use of IR-UTE sequences to detect small MS lesions in cadaver brains, as well as to measure ultrashort T_2^* values in WM both *ex vivo* and *in vivo* on a 3-T clinical scanner.[22] The reported T_2^* values (~110–330 μs) were comparable with those of myelin lipid powder when measured either alone or in a mixture with H_2O or D_2O.[22] However, because brain tissue contains different water pools (termed as long T_2 tissue components in this article) that might have different T_1 values,[5-8,23] it can be challenging to completely null water signals. Therefore, there is a possibility that the ultrashort T_2^* signals seen on IR-UTE images are contaminated by water signals.

The present study aimed to explore myelin as a source of the ultrashort T_2 signals seen in WM on IR-UTE images, and to assess the feasibility of using IR-UTE to image the ultrashort T_2 tissue components (STCs) in GM on a 3-T clinical scanner in an ovine brain D_2O exchange model. Water protons in these specimens were sequentially replaced by deuterons in D_2O. If non-exchangeable protons, such as those in myelin, are the source of the ultrashort T_2 signals seen on IR-UTE images, the measured ultrashort T_2^* value should remain constant before and after sequential D_2O exchange.

2 | MATERIALS AND METHODS

2.1 | Pulse sequences and contrast mechanisms

Figure 1 shows the two-dimensional IR-UTE pulse sequence used in this study (Figure 1A) and its contrast mechanism (Figure 1B, C). The sequence employs a half radiofrequency (RF) pulse excitation (pulse duration, 472 μs; bandwidth, ~2.7 kHz), followed by two-dimensional radial ramp sampling.[20] An initial adiabatic inversion pulse (duration, 8.64 ms; bandwidth, ~1.5 kHz) was used to invert and null the longitudinal magnetization of long T_2 tissue components. To maximize the signal-to-noise ratio (SNR) and minimize eddy currents, slice-selective gradients were turned off to image the ~3–5-mm-thick specimens used in this study.

To measure the ultrashort T_2^* signals in WM, the inversion time (TI) is chosen to null the long T_2 tissue components in WM (WM_L) (Figure 1B). At the time at which UTE acquisition starts (TE = 10 μs, i.e. $TE_{10\mu s}$), the STCs in WM (WM_S) and GM (GM_S) have positive magnetization, whereas the long T_2 tissue components in GM (GM_L) have negative magnetization. The addition of the negative magnetization from GM_L and the positive magnetization from GM_S on the $TE_{10\mu s}$ image leads to a smaller magnitude of the total GM signal, relative to that of GM_L alone. At a relatively later TE (e.g. TE = 0.6 ms, i.e. $TE_{0.6ms}$), the positive magnetization of GM_S decays to zero or near zero (so does that of WM_S), whereas the negative magnetization of GM_L decays very little. As a result, the magnitude of the total GM signal on $TE_{0.6ms}$ is nearly the same as that of GM_L alone. Consequently, subtraction of the magnitude signal on the $TE_{0.6ms}$ image from that on the $TE_{10\mu s}$ image leads to a negative signal for GM and positive signal for WM_S, i.e. WM_S is selectively imaged.

With TI chosen to null GM_L (Figure 1C), both WM_S and GM_S have positive magnetization at $TE_{10\mu s}$, which decays to zero or near zero at $TE_{0.6ms}$. WM_L has positive magnetization at $TE_{10\mu s}$, which only decays slightly at $TE_{0.6ms}$. Subtraction of the magnitude signal on the $TE_{0.6ms}$ image from that on the $TE_{10\mu s}$ image highlights both WM_S and GM_S, with WM generally showing higher signal intensity, possibly as a result of its higher myelin content than GM.[4,21]

2.2 | Ovine brain specimen preparation

Six specimens containing cerebral hemisphere (n = 5) and cerebellum (n = 1) were prepared from three freshly frozen ovine brains. All specimens were stored at 4°C and pretreated with broad-spectrum antibiotics in saline before the initial imaging (an initial image for cerebral hemisphere specimen no. 4 was not available).

Each cerebral hemisphere or cerebellum specimen (~3 mm thick) was immersed in 10 mL D_2O (99.9%, Sigma-Aldrich, St. Louis, MO, USA) in a 6.4-cm covered and sealed plastic dish to allow exchange. Four cerebral hemisphere specimens were imaged with IR-UTE sequences before and after 90-min, 150-min, 8-h and 24-h immersion intervals in D_2O (for details, please see Table 1). One cerebral hemisphere specimen was imaged with both UTE and IR-UTE sequences before and after 24 h of immersion in D_2O. The cerebellum specimen (~3 mm thick) was imaged after

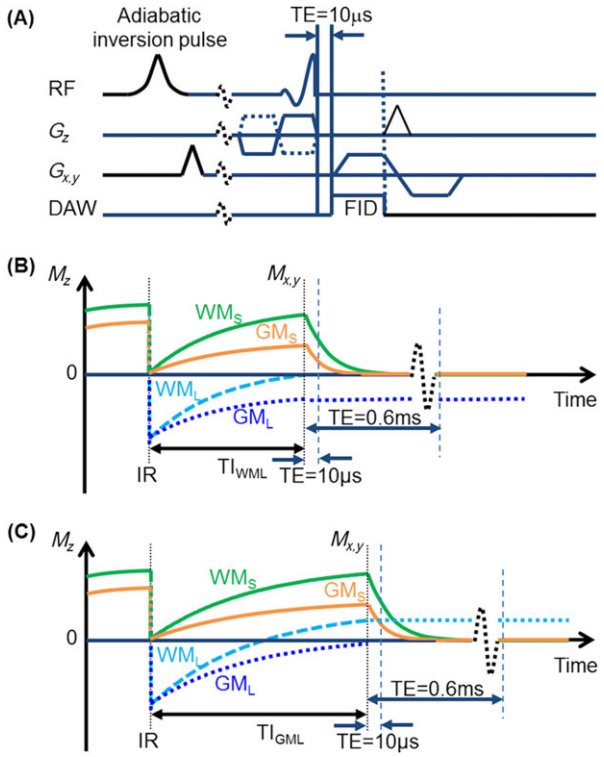

FIGURE 1 A, diagram of the two-dimensional, adiabatic, inversion recovery ultrashort echo time (IR-UTE) pulse sequence with a minimum nominal TE of 10 μs. DAW, data acquisition window; FID, free induction decay; RF, radiofrequency. (B, C) expected magnetization changes of white matter (WM) and gray matter (GM) ultrashort T_2 and long T_2 tissue components (WM_S, GM_S, WM_L and GM_L), with an inversion time (TI) that is chosen to null WM_L and GM_L, respectively. The adiabatic inversion recovery pulse provides robust inversion of the longitudinal magnetization (M_z) of long T_2 tissue components. M_z of the ultrashort T_2 tissue components experiences significant relaxation on the transverse plane during the long adiabatic inversion process, and is not inverted but partially saturated. At the time at which UTE acquisition starts (TE = 10 μs, i.E. $TE_{10\mu s}$) and with TI chosen to null WM_L B, GM_L have negative and GM_S have positive magnetization, leading to a smaller magnitude of the GM net magnetization. At a relatively longer TE (e.G. TE = 0.6 ms, i.E. $TE_{0.6ms}$), the magnitude of the GM_L signal is essentially the same as that at $TE_{10\mu s}$, whereas the WM_S and GM_S signals decay to zero or near zero. Subtraction of the magnitude signals seen in the image acquired at a longer TE from those seen on the $TE_{10\mu s}$ image provides positive contrast for WM and negative contrast for GM, enabling exclusive visualization of WM_S. With a TI chosen to null GM_L C, both WM_L and WM_S have positive signals at $TE_{10\mu s}$, and the subtraction image provides positive contrast for both WM and GM, with WM generally showing a higher signal

8-h and 32-h immersion intervals in D_2O. All specimens were allowed to reach room temperature before imaging. At each immersion time point, specimens were removed from the D_2O incubation container and flushed with fresh D_2O for 5 s prior to imaging. They were immersed in fresh D_2O again after each imaging experiment.

2.3 | Imaging experiments

All specimens were imaged using a GE 3-T Signa TwinSpeed MR scanner (GE Healthcare Technologies, Milwaukee, MI, USA) and a 7.6-cm receive-only coil. A conventional proton density-weighted fast spin echo (PD-FSE) sequence (TR/TE = 8000/13.5 ms) was used with a fixed receiver gain at all imaging time points to measure long T_2 proton signals and thereby to assess exchange between tissue protons and deuterium in D_2O. An IR-UTE sequence with TR/TE = 1000/2.2 ms and variable TIs (20, 100, 300, 500 and 800 ms) was used to determine the optimal TI for nulling long T_2 signals in WM (WM_L TI_{null}). Other parameters included a bandwidth of 166.6 kHz, a field of view (FOV) of 12 cm and an acquisition matrix of 96 × 96, providing a nominal voxel size of 0.94 × 0.94 × 3 mm^3, with a scan time of 96 s per acquisition. The same IR-UTE sequence was then used with TI = WM_L TI_{null} and variable TEs (0.01, 0.1, 0.2, 0.4, 0.6, 2 and 4 ms) to measure T_2^* of WM_S in all specimens. The T_2^* value of GM_S was also measured in the cerebellum specimen using the same IR-UTE sequence with TI set to null long T_2 signals in GM (GM_L TI_{null}). A UTE sequence without inversion preparation was performed (TR = 1000 ms; flip angle, 65°; 11 TEs ranging from 0.01 to 15 ms) in one cerebral hemisphere specimen to quantitatively estimate the fraction of STCs (f_S) before and after a 24-h immersion in D_2O.

2.4 | Data analysis

Regions of interest (ROIs) were carefully chosen in WM and GM to avoid partial volume effects. T_1 and TI_{null} were measured in each ROI offline using Matlab (Mathworks Inc., Natick, MA, USA) by fitting the IR-UTE DICOM images obtained with variable TIs using a single-component,

three-parameter fitting model. The T_2^* of STCs was quantified by fitting the IR-UTE DICOM images obtained with variable TEs using a single-component, three-parameter fitting model,[20] or fitting the UTE DICOM images with a previously reported bi-component fitting model.[24] Changes in PD-FSE signals, T_1 and T_2^* values were plotted against the immersion time in D_2O. SNR was calculated as the ratio of the mean signal intensity inside an ROI to the standard deviation of the background noise. All images shown and used for analysis were magnitude and not phase sensitive.

3 | RESULTS

Figure 2B shows representative two-dimensional IR-UTE images acquired with variable TIs (TR/TE = 1000/2.2 ms) from cerebral hemisphere specimen no. 1 before immersion in D_2O. At TI = 20 and 100 ms, there was little or no contrast between WM and GM. At TI = 300 ms, there were near-zero signals in WM and a relatively high signal in GM, suggesting dramatic suppression of signals from WM_L and insufficient suppression of signals from GM_L. At TIs of 500 and 800 ms, WM and GM signals both increased, with the WM signal being greater than that from GM. Figure 2C shows the T_1 map of WM_L and GM_L calculated from the images shown in Figure 2B. Figure 2D shows typical T_1 fitting curves for a WM ROI and a GM ROI (red boxes). TI_{null} values of ~300 and ~370 ms (TR = 1000 ms) were found for WM_L and GM_L, respectively (Figure 2D).

Figure 3A shows representative IR-UTE images with variable TEs acquired from cerebral hemisphere specimen no. 1 at WM_L TI_{null}, and the T_2^* map calculated from these images. WM had relatively lower signals than the surrounding GM, and these signals dropped progressively with the increase in TE. As shown on the T_2^* map, the WM_S T_2^* was 200–300 μs. Figure 3B shows a subtraction image (the $TE_{10\mu s}$ image minus the $TE_{0.60ms}$ image) revealing a positive signal for WM and negative signal for GM. Figure 3C shows a representative mono-exponential T_2^* fitting curve for the ROI shown in Figure 3B (yellow box).

Figure 4A shows PD-FSE images from cerebral hemisphere specimen no. 1 before and after sequential immersion in D_2O for up to 24 h. Signals progressively decreased with increasing immersion time. The SNR decreased from 166 to 11.3 in a WM ROI (the uppermost yellow box in the 0-min PD-FSE image, Figure 4A). Figure 4B shows the corresponding IR-UTE $TE_{10\mu s}$ images acquired at WM_L TI_{null}. The GM magnitude signals, arising from both short and long T_2 tissue components, progressively decreased with increasing immersion time, whereas the WM magnitude signals were relatively constant. After 24 h of immersion, the specimen, especially the WM, showed near-zero PD-FSE signals, but still had higher IR-UTE signals than the background, with an SNR of 21.4 in the abovementioned WM ROI (the uppermost yellow box in the 0-min PD-FSE image, Figure 4A). This was comparable with the SNR of the same ROI before exchange (SNR ~ 20.9). Figure 4C shows the averaged longitudinal proton density (PD) signal changes in three WM ROIs (yellow boxes in the 0-min PD-FSE image, Figure 4A). Figure 4D depicts the average T_1 changes in these ROIs. T_1 decreased from 527 ± 2 ms at baseline to 417 ± 34 ms after 24 h of immersion in D_2O. Figure 4E shows T_2^* values plotted against immersion time. As summarized in Table 1, the WM_S T_2^* values were measured to be 197 and 248 μs before and after exchange, respectively, in four cerebral hemisphere specimens.

Figure 5 shows PD-FSE (TR/TE = 8000/13.5 ms) and UTE (TR/TE = 1000/0.01 ms) images, as well as UTE bi-component T_2^* fitting results, of cerebral hemisphere specimen no. 5 before (top panel) and after (bottom panel) it was immersed in D_2O for 24 h. Like cerebral hemisphere specimen no. 1, the PD-FSE and UTE signals both dropped significantly after exchange, confirming significant exchange of H_2O with D_2O. Bi-component T_2^* analysis of the UTE images showed a very small f_S (3.8%) before exchange and an increased f_S (41%) after exchange, with an ultrashort T_2^* value constantly in the range 200–300 μs at both time points (i.e. 277 μs before exchange and 227 μs after exchange).

Figure 6A shows a PD-FSE image of the cerebellum specimen before exchange with D_2O. Figure 6B shows selected corresponding IR-UTE images acquired at variable TEs with TIs of 260 and 350 ms for nulling of WM_L and GM_L respectively. With TI = WM_L TI_{null}, the WM signal (from WM_S only) decreased and the GM signal increased with increasing TE. It should be noted that, at TE = 10 μs, GM_L and GM_S signals had negative and positive values, respectively, leading to signal cancelation. At later TEs (4 ms), GM_S signals decayed to near zero, whereas GM_L signals were largely unchanged. Therefore, the subtraction image (the $TE_{10\mu s}$ image minus the $TE_{0.6ms}$ image) showed a positive signal for WM and a negative signal for GM (Figure 6B, top panel). With TI = GM_L TI_{null}, both WM and GM signals decreased with increasing TE. The WM signal was generally higher than the GM signal. The subtraction image (the $TE_{10\mu s}$ image minus the $TE_{0.6ms}$ image) showed positive signals for both WM and GM (Figure 6B, bottom

TABLE 1 WM_S T_2^* values (μs) measured from four cerebral hemisphere specimens before and after different periods of immersion in D_2O. T_2^* was derived from mono-exponential decay fitting of IR-UTE magnitude images acquired at WM_L TI_{null} with TR = 1000 ms and a series of TEs (i.E. 0.01, 0.1, 0.2, 0.4, 0.6, 2 and 4 ms)

Specimen	0 min	90 min	150 min	8 h	24 h
1	200	215	226	n.a.	225
2	197	196	209	n.a.	n.a.
3	244	n.a.	n.a.	248	n.a.
4	n.a.	n.a.	n.a.	218	n.a.

IR-UTE, inversion recovery ultrashort echo time; n.a., not assessed; TE, echo time; TI_{null}, optimal inversion time for nulling long T_2 signals; WM_L, long T_2 tissue components in white matter; WM_S, ultrashort T_2 tissue components in white matter.

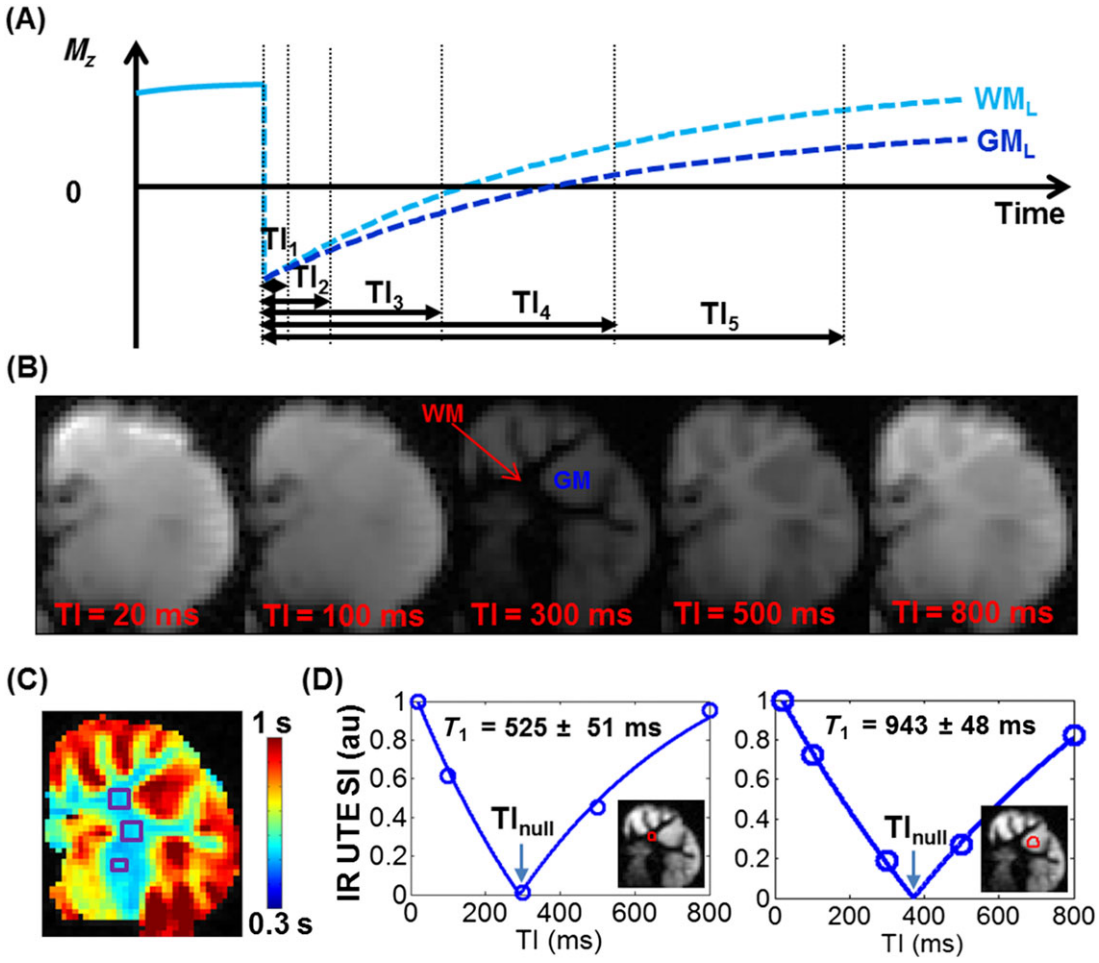

FIGURE 2 A, longitudinal magnetization (M_z) of white matter (WM) and gray matter (GM) long T_2 tissue components (i.E. WM_L and GM_L) plotted against the inversion time (TI) in the inversion recovery ultrashort echo time (IR-UTE) sequence. B, two-dimensional IR-UTE images of one cerebral specimen (no. 1) acquired with different TIs before exchange with D_2O (TR/TE = 1000/2.2 ms). It should be noted that, at TE = 2.2 ms, the signals of WM and GM ultrashort T_2 tissue components (WM_S and GM_S) become negligible because of their ultrashort T_2^* values. At shorter TIs (TI = 20 and 100 ms), there is little or no contrast between WM and GM. With TI increased to 300 ms, WM_L signals were largely suppressed and GM_L signals were moderately suppressed, as evidenced by the near-zero signals in WM and dramatic signal reduction in GM. A further increase in TI resulted in a signal increase in both WM and GM, with WM showing a higher signal than GM. C, T_1 map calculated from the images shown in (B). The three purple boxes represent three regions of interest (ROIs) defined in the WM for quantification of the average WM_L T_1. D, T_1 fitting curves of a WM ROI (left, red box) and a GM ROI (right, red box) shows that, with TR = 1000 ms, the TI for optimal nulling of long T_2 signals (TI_{null}) was ~300 ms for WM_L and ~377 ms for GM_L. SI, signal intensity

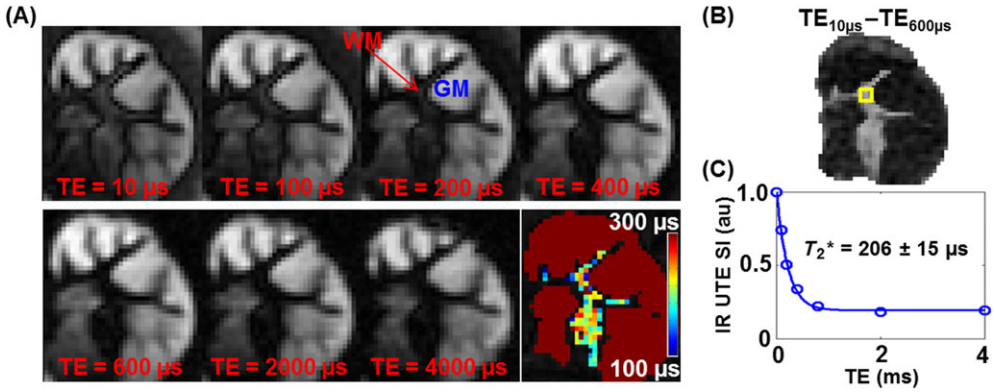

FIGURE 3 A, inversion recovery ultrashort echo time (IR-UTE) images from one cerebral specimen (no. 1) acquired before exchange with D_2O with the inversion time (300 ms) chosen to null white matter (WM) long T_2 tissue components (TR = 1000 ms). T_2^* values of WM ultrashort T_2 tissue components were 200–300 µs as shown on the T_2^* map (bottom panel, right corner). B, the magnitude subtraction image ($TE_{10µs}$ – $TE_{0.6ms}$) provides positive signal for WM and negative signal for gray matter (GM). C, mono-exponential fitting of the IR-UTE images in (a) showed a T_2^* value of 206 µs in a WM ROI (yellow box, B). SI, signal intensity

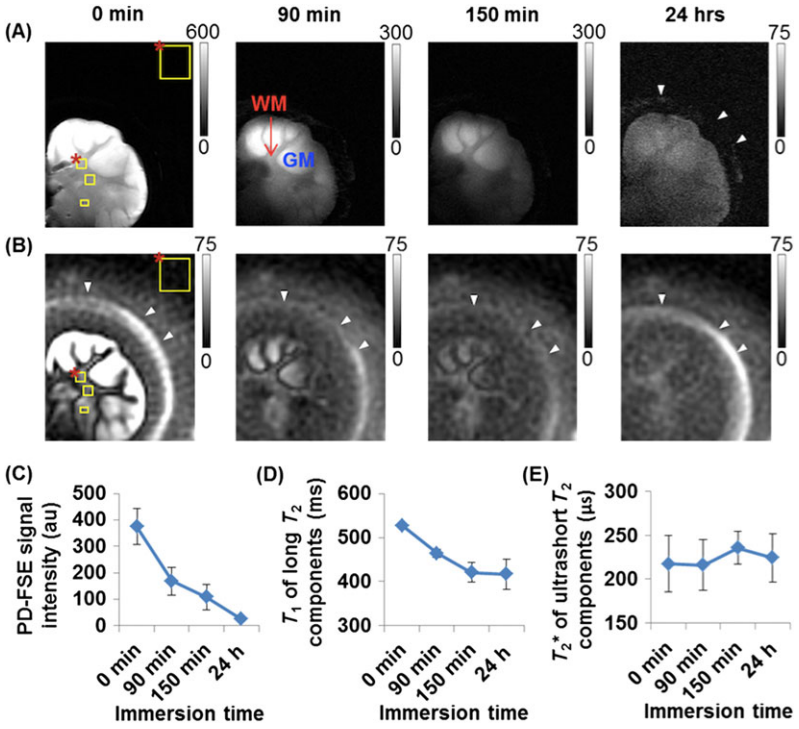

FIGURE 4 A, proton density-weighted fast spin echo (PD-FSE) images of one cerebral hemisphere specimen (no. 1) acquired before (0 min) and after sequential immersion in D_2O for 90 min, 150 min and 24 h. PD signals progressively decreased with increasing immersion time. B, corresponding inversion recovery ultrashort echo time (IR-UTE) images (TE = 10 μs) of the same specimen acquired with an inversion time that was chosen to null white matter (WM) long T_2 tissue components. C, quantitative sequential signal intensity changes of the PD-FSE images in (a), as measured in three regions of interest (ROIs) in WM (small yellow boxes inside the tissue area, 0-min PD-FSE and IR-UTE images). D, corresponding average T_1 changes in these WM ROIs. (E) relatively constant T_2^* values were obtained from these ROIs at corresponding time points. The signal-to-noise ratios (SNRs) of the PD-FSE image were 166 and 11.3 for a WM ROI (the small yellow box labeled with a red star in the 0-min PD-FSE and IR-UTE images) before and after exchange, respectively. The SNRs of the corresponding IR-UTE image were 20.5 and 21.4 before and after exchange, respectively (TE = 10 μs). White arrowheads show the margin (sealed by 3 M Micropore® surgical tape) of the 6.4-cm plastic dish containing the samples. The margin of the plastic dish was immediately next to the 7.6-cm surface coil. The ROI representing background noise was placed outside of the coil area (a, B; large yellow boxes in the top right-hand corner labeled with red stars)

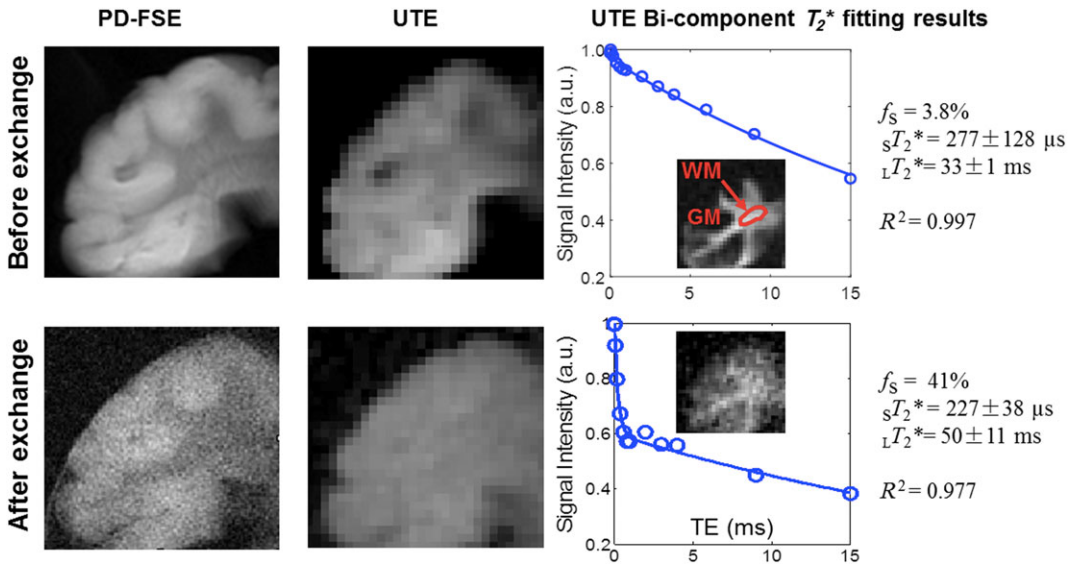

FIGURE 5 Proton density-weighted fast spin echo (PD-FSE) (TR/TE = 8000/13.5 ms) and ultrashort echo time (UTE) (TR/TE = 1000/0.01 ms) images, as well as UTE bi-component T_2^* fitting results, of one cerebral hemisphere specimen (no. 5) before (top panel) and after (bottom panel) it was immersed in D_2O for 24 h. f_S is the fraction of ultrashort T_2 tissue components, ${}_ST_2^*$ is T_2^* of the ultrashort T_2 tissue components and ${}_LT_2^*$ is T_2^* of the long T_2 tissue components. Insets in the bi-component T_2^* fitting plots are inversion recovery ultrashort echo time (IR-UTE) images (TR/TE = 1000/0.01 ms) before and after exchange with D_2O, with long T_2 signals from gray matter (GM) being suppressed by the adiabatic inversion pulse. The red circle in the top inset shows the definition of the region of interest (ROI) in white matter (WM) for T_2^* fitting at both time points

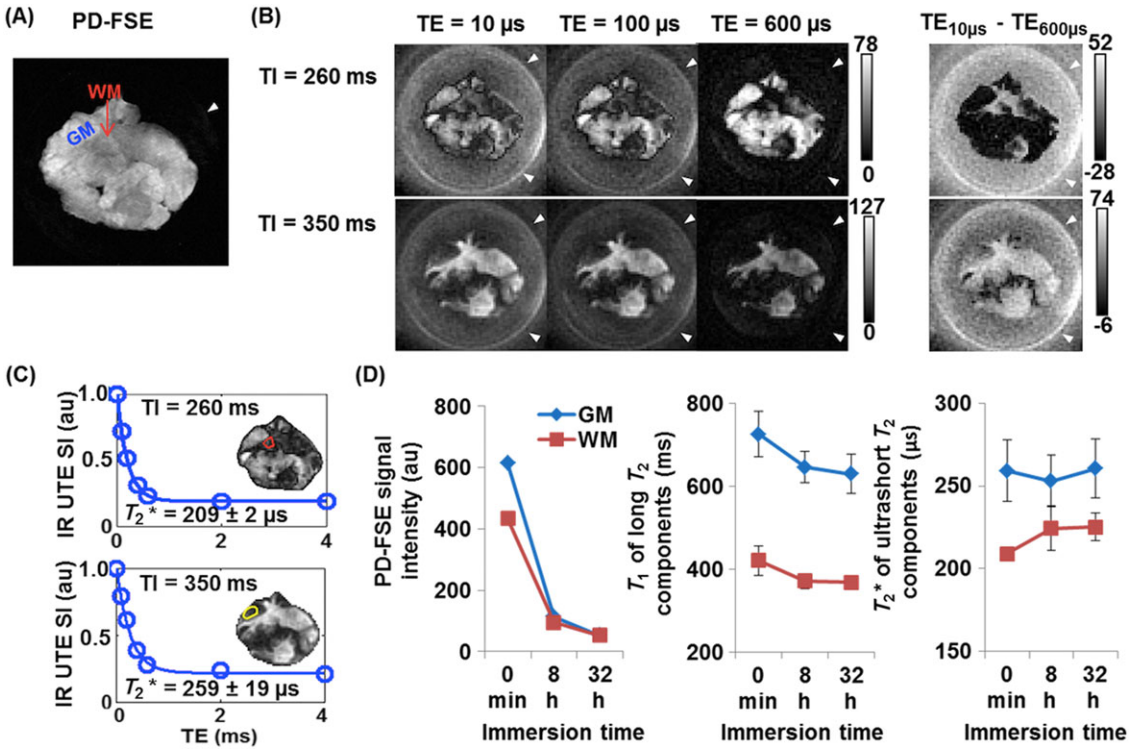

FIGURE 6 A, proton density-weighted fast spin echo (PD-FSE) image of the cerebellar specimen before exchange with D_2O. B, selected inversion recovery ultrashort echo time (IR-UTE) images of the same specimen before exchange acquired at TR = 1000 ms with two different TIs and variable TEs. At TI = 260 ms (top panel), the magnitude subtraction image ($TE_{10\mu s}$ – $TE_{0.6ms}$) highlights white matter (WM) ultrashort T_2 tissue components (WM_S). At TI = 350 ms, the subtraction image highlights both WM_S and gray matter (GM) ultrashort T_2 tissue components (GM_S), with WM_S showing a higher signal. C, T_2^* fitting curves in a WM region of interest (ROI) (TI = 260 ms, red box) and a GM ROI (TI = 350 ms, yellow circle). SI, signal intensity. D, sequential changes in average PD-FSE signal intensity, T_1 values of WM and GM long T_2 tissue components, and T_2^* values of WM_s and GM_s in the defined ROIs in (C) after immersion in D_2O. White arrowheads show the margin (sealed by 3 M Micropore® surgical tape) of the 6.4-cm plastic dish containing the samples

panel). Figure 6C shows representative T_2^* fitting curves in a WM ROI (red box in the inset) and a GM ROI (yellow box in the inset). Figure 6D plots the changes in PD-FSE signal intensity, T_1 of WM_L and GM_L, and T_2^* of WM_S and GM_S against immersion time. PD signals showed minimal differences between WM and GM after 8 h of immersion in D_2O. PD signals and T_1 of WM_L and GM_L decreased in parallel with increasing immersion time. The WM_S and GM_S T_2^* values remained relatively constant before and after exchange, with mean values of 209 ± 9 μs and 258 ± 4 μs, respectively.

4 | DISCUSSION

This study employed half-pulse IR-UTE for the first time to estimate the value of TI_{null} needed to null long T_2 water signals in the brain on a 3-T clinical scanner. Long T_2 suppression is critical for the selective imaging of myelin as water protons contribute more than 90% of the detectable UTE signal (our preliminary bi-component analysis of UTE images of fresh WM showed that only about 4% of the UTE signal has a T_2^* of ~0.3 ms, as presented in Figure 5). As suggested by the non-zero signal in the spinal cord WM on the IR-UTE image with TE/TI = 1.2/500 ms in Wilhelm et al,[2] an empirically selected TI is unlikely to be adequate for selective myelin imaging. By using the same sequence for TI_{null} estimation and T_2^* measurement, we were able to minimize potential T_1 measurement inaccuracies which could have led to insufficient nulling of long T_2 signals. This is also the most efficient method to obtain the best estimate of WM TI_{null} for the measurement of T_2^* of the STCs using IR-UTE sequences. It is simple and straightforward without requiring complicated fitting models or technically demanding corrections.

The deuterium in D_2O is an isotope of hydrogen. Its MR frequency (which scales with the gyromagnetic ratio) is 6.5 times lower than that of protons.[25] As a result, deuterium is not detectable using conventional ^1H MRI techniques. After sequential exchange with D_2O, the specimens in this study showed a gradual decrease in PD-FSE signals. The PD-FSE sequence used in this study had a TE > 10 ms and could only detect signals from long T_2 (several milliseconds or longer) tissue components. After a 24-h D_2O exchange, the specimens had near-zero long T_2 signals on the PD-FSE image, and the SNR in a WM ROI decreased by about 15-fold. The UTE signal also dropped significantly, and the bi-component T_2^* analyses showed a water fraction (relative to STCs, i.e. 1 – f_S) of approximately 59% in WM, which suggests that approximately 90% of the

WM water had been replaced by D_2O considering the innately low f_S in brain tissue. However, with TI set to TI_{null} for WM_L, SNR of the WM_S signals seen on the IR-UTE images was relatively unchanged after exchange. Furthermore, T_2^* values obtained with the IR-UTE sequence remained in the range 200–300 μs, and were independent of the duration of exchange. The ${}_ST_2^*$ values obtained with bi-component T_2^* analysis of the UTE images were also constantly in the range 200–300 μs before and after D_2O exchange. These T_2^* values were comparable with those measured in myelin extract powder, as well as in mixtures of the powder with D_2O and H_2O using the IR-UTE sequence in one previous study.[22] Despite the incomplete H_2O/D_2O exchange in the present ovine brain D_2O exchange model, our results suggest a minimal contribution from exchangeable long T_2 protons to the ultrashort T_2^* signals seen on IR-UTE images acquired both before and after D_2O exchange. These results support the view that the ultrashort T_2^* signals seen on IR-UTE images are unlikely to be generated from water or residual water in the tissue. They are more likely to be associated with non-aqueous protons.

The STC-invisible PD-FSE images always showed higher signal in GM and lower signal in WM, suggesting that there was more long T_2 water in GM than in WM both before and after D_2O exchange (Figures 4 and 5). Like the PD-FSE images, the UTE images (TR = 1000 ms) acquired at an ultrashort TE (TE = 0.01 ms) were also mainly PD weighted. As a result of the large FA used (FA = 65°), the UTE image also showed T_1 weighting, leading to a higher signal in WM than in GM (if there was no difference in PD) because WM_L had a shorter T_1 than GM_L (Figures 2D, 6D). Unlike the PD-FSE image, the 'STC-sensitive' UTE image showed weaker WM/GM contrast before D_2O exchange and largely no WM/GM contrast after D_2O exchange (Figure 5). This can be explained as follows. In fresh brain tissue, GM had a higher water PD than WM, and WM had a higher non-aqueous PD than GM.[1,2,4] The total number of protons, including all water protons and solid mass protons, might not be significantly different between WM and GM.[26] However, not all of the solid mass proton signals were detectable with the UTE sequence with a TE of 0.01 ms.[2] Therefore, the WM/GM contrast induced by the water content difference might not be completely canceled by the WM/GM non-aqueous proton content difference and the T_1 weighting of the UTE sequence, leading to a higher signal in GM than in WM on the UTE image (Figure 5B). After 24-h D_2O exchange, the signal on the PD-FSE image dropped by ~90%, suggesting significant exchange of H_2O with D_2O (Figure 5A, D). The PD-FSE image still showed higher signal in GM than in WM, suggesting that there was more residual water in GM than in WM after 24-h D_2O exchange (Figure 5D), but the absolute WM/GM water PD difference should be much smaller than that before D_2O exchange. Meanwhile, methylene protons in the brain non-aqueous tissue are thought to be the major non-exchangeable protons in nervous tissue.[4] As a result, the difference between WM/GM non-aqueous PDs was largely reserved after D_2O exchange. In addition, WM_L still had a shorter T_1 than GM_L after D_2O exchange (Figure 6D). These factors, altogether, could have made the contrast between WM and GM undiscernible on the UTE image after D_2O exchange. Because of the presence of residual water, the WM/GM contrast on the IR-UTE images after incomplete D_2O exchange was affected by many factors. These factors included the differences in the amount of WM/GM residual water and T_1 values of WM_L and GM_L, the difference in the total number of non-exchangeable protons in WM and WM, and potential T_1 differences of the WM/GM STCs (which needs further investigation).

GM_S also showed ultrashort submillisecond T_2^* values, which were slightly but consistently higher than those of WM_S in the same specimen at all imaging time points and, like WM_S, showed minimal change with increasing immersion time in D_2O. The ultrashort T_2^* signals seen in nerve tissues and bovine brain myelin extract after D_2O exchange are thought to predominantly arise from carbon-bound methylene protons.[4] However, methylene protons also exist in other non-myelin membranous structures of cells.[27] Because GM contains more cellular and subcellular structures than WM, GM_S might be composed of a much higher fraction of other methylene-containing macromolecules than myelin. Protons in these macromolecules might have different T_2^* values from those in myelin, which warrants more sophisticated investigation with a larger sample size and the analysis of different WM and GM regions. The IR-UTE sequences may therefore have applications in the characterization of GM abnormalities, and the characterization of GM_S may also potentially provide an important biomarker for MS.[28]

The T_1 values of GM_L and WM_L varied significantly with increasing immersion time in D_2O; therefore, a wide range of TIs (240–330 ms for WM and 320–350 ms for GM) were used to null signals from these components. The T_1 decrease with D_2O exchange may be a result of gradual tissue water loss. In native tissue, the fast-relaxing non-aqueous protons would accelerate T_1 relaxation of aqueous protons through magnetization transfer.[29] In deuterated tissue, the ratio of exchangeable aqueous protons to non-exchangeable non-aqueous protons was greatly reduced. The magnetization transfer effects could be more prominent and lead to further reduced T_1 of the residual aqueous protons. Another possibility is that the relatively free water might be first replaced by D_2O; the remaining signal on IR-UTE images would be dominated by bound water, such as that trapped in macromolecules, and could have a relatively short T_1.[5,23] Prolonged D_2O exchange for up to 7 days led to a T_1 increase (data not shown here), possibly because of a loss of macromolecular peptides as a result of tissue degeneration.[30] The T_2^* values remained relatively constant despite changes in T_1 of GM_L and WM_L.

There are several limitations of this study. First, in a clinical setting with slice-selective gradients switched on, eddy currents, which occur commonly with MRI scanners, can cause distortion of the combined *k*-space signal profile. This was not investigated in this study. If strong eddy currents exist, it might be necessary to take measures, such as dedicated prescans, to mitigate against this problem.[31] Second, different forms of tissue water may have different exchange rates with D_2O. This was not explored in this study. Nevertheless, the relatively constant T_2^*values suggest minimal water contamination in the IR-UTE T_2^* measurements. Third, myelin T_1 and PD were not measured. It is possible to probe the fraction of exchangeable myelin protons by comparing the IR-UTE signals before and after D_2O exchange. This needs T_1 correction as the T_1 value of myelin protons may change significantly in a deuterated environment, and this warrants further investigation. Last, although this study was performed within 32 h of tissue thawing, the specimens may still have undergone natural degradation and their myelin properties might have changed after D_2O exchange. Histology is required in future studies for the assessment of any such effect.

5 | CONCLUSION

In conclusion, our results suggest that the IR-UTE sequence can be applied on a clinical scanner to directly detect signals from non-aqueous protons, presumably myelin protons in WM, as well as protons in other STCs in GM. This requires an accurate estimation of WM_L and GM_L TI_{null} values, which can be determined by fitting the IR-UTE images acquired with variable TIs to a standard single-component T_1 measurement fitting model. This technique can also be used to measure myelin T_1 and PD. Such quantitative measures may provide a new opportunity to characterize demyelinating diseases.

ACKNOWLEDGEMENTS

This study was supported by National Institute of Neurological Disorders and Stroke, National Institutes of Health (NINDS, NIH) (1R01 NS092650).

REFERENCES

1. Laule C, Vavasour IM, Kolind SH, et al. Magnetic resonance imaging of myelin. *Neurotherapeutics*. 2007;4(3):460-484.
2. Wilhelm MJ, Ong HH, Wehrli SL, et al. Direct magnetic resonance detection of myelin and prospects for quantitative imaging of myelin density. *Proc Natl Acad Sci U S A*. 2012;109(24):9605-9610.
3. Koch-Henriksen N, Sorensen PS. The changing demographic pattern of multiple sclerosis epidemiology. *Lancet Neurol*. 2010;9(5):520-532.
4. Horch RA, Gore JC, Does MD. Origins of the ultrashort-T2 ^{1}H NMR signals in myelinated nerve: a direct measure of myelin content? *Magn Reson Med*. 2011;66(1):24-31.
5. Deoni SCL, Rutt BK, Arun T, Pierpaoli C, Jones DK. Gleaning multicomponent T(1) and T(2) information from steady-state imaging data. *Magn Reson Med*. 2008;60(6):1372-1387.
6. Bjarnason TA, Vavasour IM, Chia CLL, MacKay AL. Characterization of the NMR behavior of white matter in bovine brain. *Magn Reson Med*. 2005;54(5):1072-1081.
7. MacKay A, Laule C, Vavasour I, Bjarnason T, Kolind S, Madler B. Insights into brain microstructure from the T2 distribution. *Magn Reson Imaging*. 2006;24(4):515-525.
8. Whittall KP, MacKay AL, Graeb DA, Nugent RA, Li DK, Paty DW. In vivo measurement of T2 distributions and water contents in normal human brain. *Magn Reson Med*. 1997;37(1):34-43.
9. Schmierer K, Scaravilli F, Altmann DR, Barker GJ, Miller DH. Magnetization transfer ratio and myelin in postmortem multiple sclerosis brain. *Ann Neurol*. 2004;56(3):407-415.
10. Gareau PJ, Rutt BK, Karlik SJ, Mitchell JR. Magnetization transfer and multicomponent T2 relaxation measurements with histopathologic correlation in an experimental model of MS. *J Magn Reson Imaging*. 2000;11(6):586-595.
11. Tomiak MM, Rosenblum JD, Prager JM, Metz CE. Magnetization transfer: a potential method to determine the age of multiple sclerosis lesions. *Am J Neuroradiol*. 1994;15(8):1569-1574.
12. Rovaris M, Judica E, Sastre-Garriga J, et al. Large-scale, multicentre, quantitative MRI study of brain and cord damage in primary progressive multiple sclerosis. *Mult Scler*. 2008;14(4):455-464.
13. Ramani A, Aliev AE, Barker GJ, Tofts PS. Another approach to protons with constricted mobility in white matter: pilot studies using wideline and high-resolution NMR spectroscopy. *Magn Reson Imaging*. 2003;21(9):1039-1043.
14. Lancaster JL, Andrews T, Hardies LJ, Dodd S, Fox PT. Three-pool model of white matter. *J Magn Reson Imaging*. 2003;17(1):1-10.
15. Filippi M, Rocca MA. MR imaging of multiple sclerosis. *Radiology*. 2011;259(3):659-681.
16. Kappos L, Moeri D, Radue EW, et al. Predictive value of gadolinium-enhanced magnetic resonance imaging for relapse rate and changes in disability or impairment in multiple sclerosis: a meta-analysis. Gadolinium MRI Meta-analysis Group. *Lancet*. 1999;353(9157):964-969.
17. Bakshi R, Thompson AJ, Rocca MA, et al. MRI in multiple sclerosis: current status and future prospects. *Lancet Neurol*. 2008;7(7):615-625.
18. Milo R, Kahana E. Multiple sclerosis: geoepidemiology, genetics and the environment. *Autoimmun Rev*. 2010;9(5):A387-A394.
19. Schmierer K, Wheeler-Kingshott CA, Tozer DJ, et al. Quantitative magnetic resonance of postmortem multiple sclerosis brain before and after fixation. *Magn Reson Med*. 2008;59(2):268-277.
20. Du J, Ma GL, Li SH, et al. Ultrashort echo time (UTE) magnetic resonance imaging of the short T2 components in white matter of the brain using a clinical 3T scanner. *Neuroimage*. 2014;87:32-41.
21. Waldman A, Rees JH, Brock CS, Robson MD, Gatehouse PD, Bydder GM. MRI of the brain with ultra-short echo-time pulse sequences. *Neuroradiology*. 2003;45(12):887-892.
22. Sheth V, Shao H, Chen J, et al. Magnetic resonance imaging of myelin using ultrashort echo time (UTE) pulse sequences: phantom, specimen, volunteer and multiple sclerosis patient studies. *Neuroimage*. 2016;136:37-44.
23. Does MD, Gore JC. Compartmental study of T(1) and T(2) in rat brain and trigeminal nerve in vivo. *Magn Reson Med*. 2002;47(2):274-283.
24. Li S, Ma L, Chang EY, et al. Effects of inversion time on inversion recovery prepared ultrashort echo time (IR-UTE) imaging of bound and pore water in cortical bone. *NMR Biomed*. 2015;28(1):70-78.
25. Muller S, Seelig J. In vivo NMR imaging of deuterium. *J Magn Reson*. 1987;72(3):456-466.
26. Tofts P. *Quantitative MRI of the Brain: Measuring Changes Caused by Disease*. New York: Wiley; 2003.
27. Bloom M, Holmes KT, Mountford CE, Williams PG. Complete proton magnetic-resonance in whole cells. *J Magn Reson*. 1986;69(1):73-91.
28. Yarnykh VL, Bowen JD, Samsonov A, et al. Fast whole-brain three-dimensional macromolecular proton fraction mapping in multiple sclerosis. *Radiology*. 2015;274(1):210-220.
29. van Gelderen P, Jiang X, Duyn JH. Effects of magnetization transfer on T1 contrast in human brain white matter. *Neuroimage*. 2016;128:85-95.

30. De Guio F, Reyes S, Duering M, Pirpamer L, Chabriat H, Jouvent E. Decreased T1 contrast between gray matter and normal-appearing white matter in CADASIL. *Am J Neuroradiol*. 2014;35(1):72-76.

31. Abe T. Half radiofrequency pulse excitation with a dedicated prescan to correct eddy current effect and gradient delay. *Med Phys*. 2013;40(3): 032304.

How to cite this article: Fan S-J, Ma Y, Chang EY, Bydder GM, Du J. Inversion recovery ultrashort echo time imaging of ultrashort T_2 tissue components in ovine brain at 3 T: a sequential D_2O exchange study. *NMR in Biomedicine*. 2017;30:e3767. https://doi.org/10.1002/nbm.3767